PROCEEDINGS OF SPIE

Wafer scale FeCl$_3$ intercalated graphene electrodes for photovoltaic applications

Kieran K. Walsh, Conor Murphy, Gareth Jones, Matthew Barnes, Adolfo De Sanctis, et al.

SPIE.

Wafer Scale FeCl₃ Intercalated Graphene Electrodes For Photovoltaic Applications

Kieran K. Walsh[a], Conor Murphy[a], Gareth Jones[a], Matthew Barnes[a], Adolfo De Sanctis[a], Shin Dong-Wook[a], Saverio Russo[a], and Monica Craciun[a]

[a]Centre for Graphene Science, College of Engineering, Mathematics and Physical Sciences, University of Exeter, Exeter EX4 4QF, United Kingdom.

ABSTRACT

The alteration of graphene's electrical properties through chemical functionalization is a necessary process in order for graphene to fulfill its potential as a transparent conducting electrode. In this work, we present a method for the transfer and intercalation of large area (wafer scale) graphene samples to produce highly doped FeCl₃ intercalated Few Layer Graphene (FeCl₃-FLG). Given its excellent flexibility, transmission, and a sheet resistance, comparable to that of Indium Tin Oxide, FeCl₃-FLG has potential to replace alternative flexible transparent electrodes as well as compete with rigid transparent electrodes. We assess the effect of functionalization temperature on the degree of intercalation in the large area samples and comparing results to that of 1 cm² FeCl₃-FLG samples. Raman spectroscopy is then used to characterize samples, where we introduce a new figure of merit ($\langle \text{PosG} \rangle$) by which to assess the degree of intercalation in a sample. This is an average G peak position, weighted by the areas of the constituent peaks, which can then be used to map the charge carrier concentration of the sample. The inhomogeneity of the graphene grown by chemical vapor deposition is found to be one of the limiting factors in producing large area, high quality FeCl₃-FLG.

Keywords: Graphene, Intercalated, FeCl₃, Large Area, Flexible, Electrode

1. INTRODUCTION

In recent years, there has been a renewed interest into photovoltaic technologies due to their appealing ability to reliably produce energy only using sunlight, without the production of any unwanted greenhouse gases. Combine this with the discovery of 2 dimensional (2D) materials, and it comes as little surprise that the application of 2D materials in photovoltaic devices is currently such a popular area of study. This ranges from the use of transition metal dichalcogenides as the photoactive layers in devices, forming atomically thin p-n junctions,[1–3] to investigations into graphene as a potential material for use as electrodes.[4, 5] The electrode is responsible for the collection and transport of charge away from the photoactive region of the device. This not only requires the material used to have a high conductivity in order to efficiently transport the electrical current produced by the photovoltaic device, but also to be transparent across the visible spectrum such that fewer photons are absorbed before reaching the p-n junction and producing free charge carriers. Indium Tin Oxide (ITO) has long been the market standard for use as a transparent conducting electrode, due to its low sheet resistance and high optical transparency. However, recent evidence has shown ITO to have a high energy cost in production,[6] as well as many reports of device degradation being caused by Indium diffusion to the photoactive region.[7, 8] This shows the need for an alternative material that requires a less costly manufacturing process, made from easily available, non-toxic chemicals. Graphene would appear to be the ideal candidate for a transparent conducting electrode, owing to its high optical transparency (2.3 % for a single layer[9]) and fantastic electron transport properties. In addition, graphene is flexible, opening possibilities for flexible solar cell technologies to be developed. However, early research revealed graphene's sheet resistance ($\approx$1 kΩ/sq) lead to reduced device efficiencies compared to that of ITO. In addition, much of the research currently conducted focuses only graphene flakes exfoliated from graphite crystals. This misrepresents the potential of graphene technology, as the high quality of graphene that is produced through exfoliation cannot be replicated on the larger scale using graphene produced by Chemical

---

Vapor Deposition (CVD) or solution processing. To produce electrodes that have potential for use in full-scale devises, CVD graphene is the best candidate due to its optical transparency and compatibility with roll-to-roll processing techniques. However, due to the aforementioned high sheet resistance, the graphene must first be functionalized to improve its conductive properties.

One alternative to graphene is $FeCl_3$ intercalated Few Layer Graphene ($FeCl_3$-FLG),[10] a heavily doped form of Few Layer Graphene (FLG) produced through intercalation of graphene with $FeCl_3$. Intercalation is a process by which atomic or molecular species fill the spaces in a layered structure. In the case of $FeCl_3$-FLG, this involves the atomic sheets of carbon separating to allow $FeCl_3$ molecules to fill the space between the layers.[11] It has been shown that intercalation with $FeCl_3$ causes strong charge transfer from the graphene to the $FeCl_3$, leading to a high level of hole doping in the graphene sheets.[12] This dramatically increases the charge carrier concentration and consequently reduces the sheet resistance to as low as 8 Ω/sq, while maintaining graphene's high transmission across the visible and infra-red spectra.[10] Previous studies have shown $FeCl_3$-FLG to offer improved performance compared to other flexible transparent electrodes, such as PEDOT-PSS. However, the size of these devices was limited to about 9 cm^2, preventing the technology from being scaled up for testing in full-scale devices. Here, we report an improved automated transfer method, based around a custom-built mount, and intercalation procedure capable of fabricating $FeCl_3$-FLG samples as large as 36 cm^2. Furthermore, we propose a new metric by which to characterize these large area samples by Raman spectroscopy, that is more representative of the material's properties than those used in previous studies.[12] This provides the opportunity to investigate the potential improvements in efficiency that $FeCl_3$-FLG can provide in much larger scale devices.

2. METHODS

4 inch wafers grown by Chemical Vapor Deposition (CVD) were purchased from Graphene Supermarket. On these wafers the graphene was grown on a thin layer of Nickel catalyst, on top of a Si/SiO_2 wafer, and was characterized as having 98% coverage of 1-7 layers. A Polymethylmethacrylate (PMMA, A4 495k) protective layer was then spin coated onto the wafer (7000 rpm). This layer provides protection from surface contamination and physical damage to the graphene, as well as aiding flotation during the etching stage of transfer. The wafer was then scribed and cut to size in preparation for etching and transfer. Glass substrates were cleaned by sonication in Deionised water (DI water) for 10 minutes, followed by rinsing in Acetone and Isopropyl Alcohol (IPA) for 10 minutes each, and at 70°C. Substrates were then plasma cleaned in an oxygen plasma using a JLS RIE80, this ensures a clean surface for graphene transfer and aids adhesion of the graphene film to the glass substrate.

2.1 Graphene Transfer

Etching and transfer took place on a custom built wedge placed in an etching bath where the graphene wafer was mounted and fixed in place using a small amount of PMMA. 0.5 Molar $FeCl_3$ solution was then flooded into the bath until it reached the bottom edge of the wafer and etching could begin. $FeCl_3$ will etch the Nickel from underneath the graphene film, separating it from the Si/SiO_2 wafer and allowing the graphene to float on the surface. A pair of peristaltic pumps were used to control the flow rate of $FeCl_3$ solution via a piece of software that allowed them to pump continuously for 2 seconds every minute. This periodic flow rate of $FeCl_3$ into the etching bath allowed the $FeCl_3$ to etch the Nickel from underneath the graphene film without causing any folds, wrinkles or tears in the graphene film. In this manner, the rate of etching could be controlled with minimal participation from the researcher while ensuring no additional defects would be introduced into the graphene film. Once the $FeCl_3$ had etched the entire graphene film, the pumps were set to continually pump water into the etching bath. This would flood the bath and lower the concentration of the $FeCl_3$ solution until it was visibly clear. The bath was then flooded with DI water for a further hour to ensure any traces of $FeCl_3$ had been washed away. This ensures minimal contamination from $FeCl_3$ particles under the film's surface, which can cause aggregation of $FeCl_3$ during the intercalation process. The Si/SiO_2 wafer is then carefully removed from under the graphene film and replaced with the clean glass substrate. The pumps are then used to drain the bath, allowing the graphene film to slowly cover the clean glass substrate. Once the bath is completely drained, the graphene sample is removed and allowed to air dry before being post baked at 120°C for 10 minutes to improve adhesion to the substrate. The PMMA layer is then washed off in Acetone (70°C, 2 hours) and the sample is desiccated.
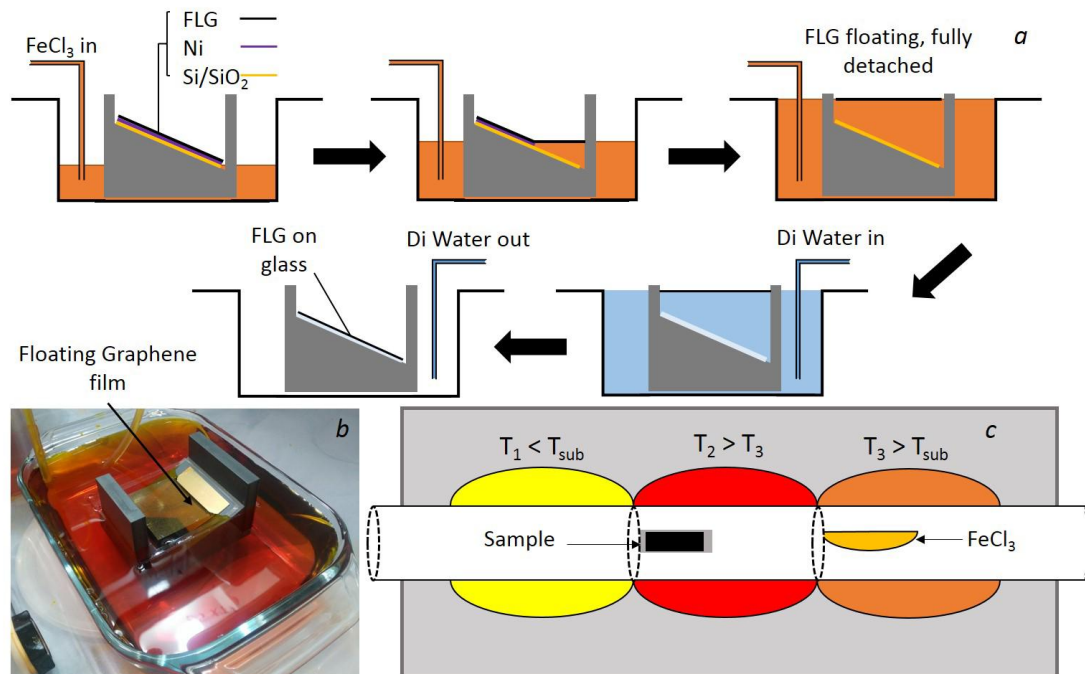
Figure 1: **a**: Graphene transfer process for large area samples. The wedge holds the sample in place as FeCl$_3$ solution is used to etch away the graphene, DI water is then pumped into the bath and the substrate replaced with a clean glass substrate, before the bath is drained to complete the transfer process. **b**: Image of the transfer setup during the etching of a 6x6 cm sample of graphene, seen floating on the surface of the FeCl$_3$ solution. **c**: Diagram of intercalation furnace, where T$_2$ and T$_3$ are greater than the temperature of sublimation for FeCl$_3$, and T$_1$ is less. T$_2$ is kept higher than both T$_1$ and T$_3$ so as to create a temperature gradient away from the sample in the tube, this helps to maintain a clean sample at the end of intercalation.

2.2 Intercalation

Intercalation took place inside a quartz tube within a three zone furnace, the graphene sample was placed in zone 2, while a vial of anhydrous FeCl$_3$ was placed in zone 3. The tube was then evacuated down to a pressure of 1×10^{-6} mbar and the heating procedure was started, heating each zone to its target temperature at a rate of $10°$C s^{-1}. The sample and FeCl$_3$ were heated to $360°$C and $315°$C respectively, while the left zone was heated to $300°$C to prevent condensation of FeCl$_3$ on the sample. After 12 hours of intercalation the chamber was evacuated before being vented, and the sample removed. FeCl$_3$-FLG samples were then desiccated for 24 hours and washed in IPA ($70°$C for 10 minutes) to remove traces of Iron Oxide contaminants on the surface before Raman characterization.

2.3 Raman Characterization

Raman spectroscopy was carried out on a custom built multipurpose microscope, specifically made for the characterization of optoelectronic devices made from 2D materials.[13] A 5 mW, 514 nm laser was used, with a 2 second exposure time. Typically, Raman maps were taken over a 30x30 μm area with a 1 μm step size. Larger maps (300x300 μm) were also taken to characterize large areas of the samples by periodically sampling point spectra from flakes with a 10 μm step size. This provides a more representative insight into the doping of the FeCl$_3$-FLG film, as the sampling will be unaffected by local variation in flake thickness as well as any holes present in the film. The Raman maps were analyzed using a Matlab script written for that purpose, fitting Lorentzian functions to the G$_0$, G$_1$ and G$_2$ peaks found in FeCl$_3$ intercalated graphene. This allows the calculation of the $\langle$PosG$\rangle$ value figure of merit as well as the estimation of charge density following the model developed by *Lazzeri et al.*[14]
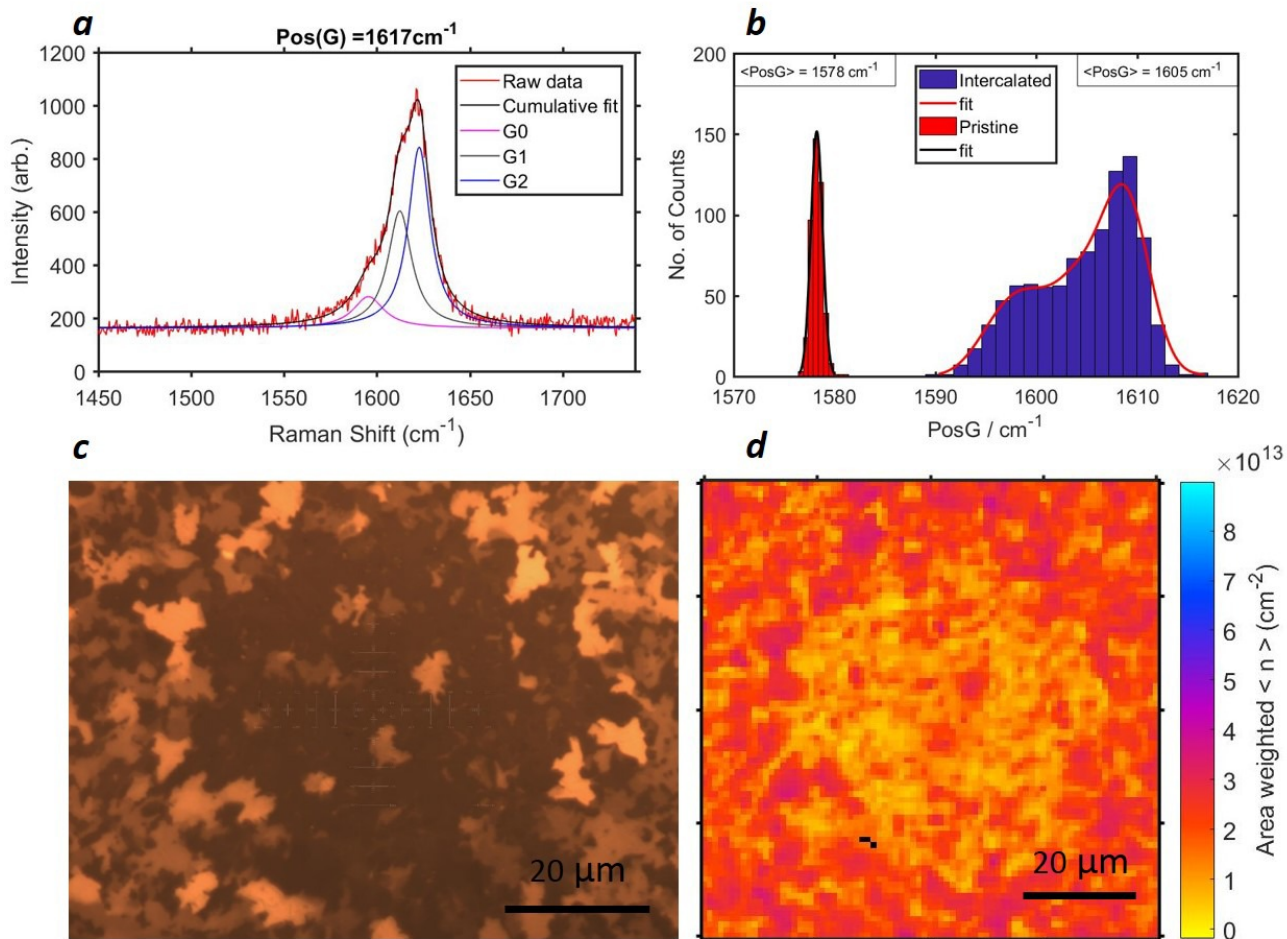
Figure 2: **a**: Raman Spectrum of a stage 2 intercalated flake from a large area sample, displaying a PosG value of 1617 cm^{-1}. Lorentzian fits to the G_0, $G1_1$ and G_2 constituent peaks are shown. **b**: Histograms for large area samples showing the shift in PosG distribution before and after intercalation. **c**: Optical image of a hole in a large area FeCl$_3$-FLG sample. **d** Charge carrier concentration map of the same area as in **c**. Charge carrier concentration calculated using the work of *Lazeri et. al.*[14] and the PosG metric

2.4 Sheet Resistance Measurements

Once samples had been characterized through Raman spectroscopy, sheet resistance (Rs) measurements were taken using a linear 4 point probe setup, sourcing a current between the two outer probes and measuring the voltage between the two inner probes. 1x1 cm sections were cut into the films to control the geometry of the sample, 9 resistance measurements were then taken in different areas of the 1x1 cm section to account for local variations in FeCl$_3$-FLG quality. These measurements were then averaged and used to calculate the sheet resistance.

3. RESULTS AND DISCUSSION

Samples as large as 36 cm^2 were transferred and intercalated using the method outlined above. The intercalation of graphene with FeCl$_3$ causes a strong charge transfer from the graphene to the FeCl$_3$, due to the strong overlap of delocalised p-orbitals in graphene with the d-orbitals of the Iron in FeCl$_3$ molecules.[15] This is detected through a positive shift in the G-peak position in the Raman spectrum of graphene, due to the stiffening of the E_{2g} phonon mode on account of the removal of the Kohn anomaly.[14] This relates to a shift in the Fermi energy in

the graphene, caused by the positive hole doping. It has been reported that the G-peak position directly relates to the number of adjacent $FeCl_3$ layers doping the graphene flake at that location in the sample and hence the level of doping. This splits the G-peak into three constituent peaks called G_0, G_1 and G_2 peaks respectively. An undoped flake has a corresponding G_0-peak position of 1580 cm^{-1}, a sheet adjacent to a single $FeCl_3$ layer has a corresponding G_1-peak at 1612 cm^{-1} and a sheet doped on either side by $FeCl_3$ has a corresponding G_2-peak at 1625 cm^{-1}. Depending on the number of layers and the doping configuration of each graphene flake, these peaks will vary in intensity. This presents a problem to those wishing to characterize large area samples by Raman spectroscopy, due to the variation in the flake size and thickness in CVD graphene. This inhomogeneous nature of CVD graphene means that, when intercalated, the degree of intercalation, as well as the staging are highly dependent on location across the sample. To overcome this obstacle to characterization, we propose a new metric by which to measure the chemical doping in graphene, that takes into account both peak position and intensity for each of the constituent G peaks. This area weighted G-peak position, ⟨PosG⟩, calculates the average G-peak position by summing the position of the G_0, G_1 and G_2 peaks weighted by their area and then normalizing this value to the total area of the G-peak, as shown by equation(1).

$$< PosG >= \frac{PosG_0 \frac{AreaG_0}{2} + PosG_2 AreaG_2 + PosG_3 AreaG_3}{\frac{AreaG_0}{2} + AreaG_1 + AreaG_2}, \tag{1}$$

where $PosG$ refers to the Raman shift position of that respective peak in cm^{-1} and $AreaG$ is the Area of that respective peak. The factor of $1/2$ in the $AreaG_0$ terms originates from the reduction in Full Width at Half Maximum (FWHM) of the G peak by approximately $1/2$ due to increasing the charge carrier concentration to $\approx 3 \times 10^{13}$ cm^{-2}.[16] This allows the average Raman G-peak position to be displayed on a single map, rather than 3 separate maps (one for each G-peak) as has been presented in the past.[12] This metric also provides better insight into the doping conditions in the graphene sheets, by correlating the charge carrier concentration calculated from the ⟨PosG⟩ value with optical images of the $FeCl_3$-FLG sample it can be seen how the doping, and hence intercalation, varies with the thickness of each flake as well as the density of flakes in the film.

Fabrication of large area samples also requires a larger intercalation tube than used in previous investigations. Changing the size of the tube also requires adjustment of intercalation conditions, as it was discovered that the conditions used for intercalation in a 3 cm diameter tube did not lead to successful intercalation in a 9 cm diameter tube. The temperature of the intercalant zone was varied from $300 - 360°$C in order to adjust the vapor pressure of the $FeCl_3$ vapor during intercalation. This is thought to have an effect on the quality of intercalation as $FeCl_3$ molecules will be able to more easily penetrate the graphene layers at a higher pressure. Results show that increasing the intercalant zone temperature from the previously used temperature of $315°$C, to $360°$C caused an increase in the ⟨PosG⟩ value from approximately 1590 cm^{-1} to 1603 cm^{-1}. Although this value is lower than that quoted for stage 2 intercalated graphene's G_1 peak, because this metric takes into account the position of all peaks, as well as the area ratio between them, it can be shown that a ⟨PosG⟩ value of 1603 cm^{-1} actually relates to a G-peak with G_0, G_1 and G_2 sub-peaks present. This shows that some of the flakes present in the graphene film fully intercalate, while others do not. Figure 2.b shows the distribution of PosG measurements made on intercalated and unintercalated samples. It can be seen that the histograms do not overlap, demonstrating that after intercalation all flakes are at least partially doped compared to an unintercalated sample. Figure 2.d shows a charge carrier concentration map produced from a Raman map of a hole in the sample. When compared to the optical image of the same area of $FeCl_3$-FLG (2.c), it can be seen that the center of the hole is covered in doped graphene with a lower charge carrier concentration than outside of the hole. This is because Nickel grown CVD graphene forms a continuous bilayer of graphene underneath the islands of FLG on the surface.[17] This bilayer is particularly difficult to intercalate due to the lack of edges in the continuous film. Thicker flakes surrounding the hole possess 2–4 times the charge carrier concentration as the partially doped bilayer, highlighting the need for high quality, homogeneous CVD graphene for the production of uniformly doped $FeCl_3$-FLG.

The variation in flake coverage in our samples means that direct maps do not guarantee a representative measurement of the doping conditions across the whole sample. It is therefore necessary to map a larger area of the sample and periodically sample points from within that area to take Raman spectra from. This allows the calculation of a statistically representative ⟨PosG⟩ that will account for this variation in doping conditions. As
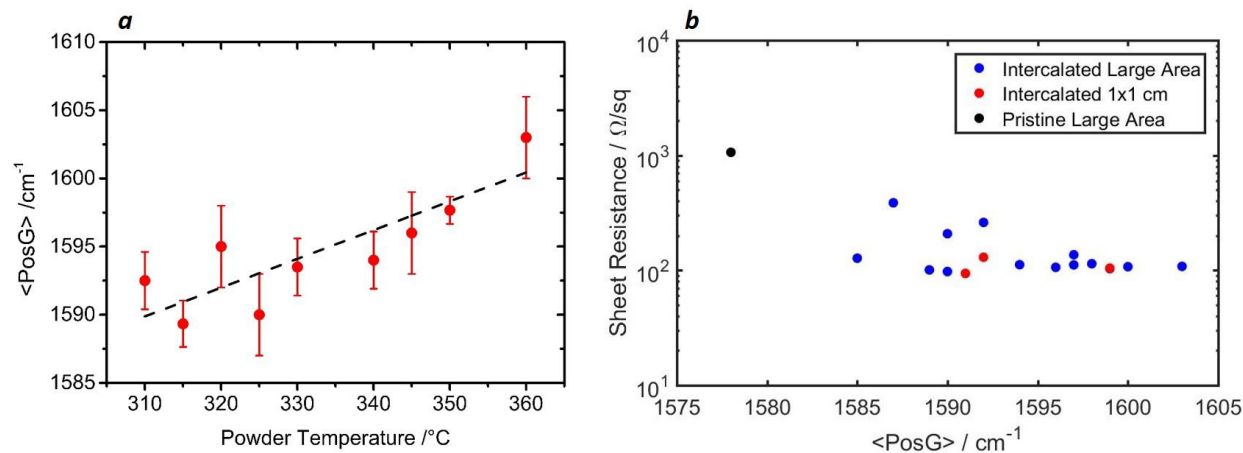
Figure 3: **a**: Variation in $\langle PosG \rangle$ with increasing intercalant powder temperature for large area samples. **b**: Sheet resistance of $FeCl_3$-FLG samples. Large area samples are shown to attain the same sheet resistance as smaller samples of higher quality.

such, a point sampling method was employed, where a much larger map (300x300 μm) was taken but only every tenth point sampled. The $\langle PosG \rangle$ value calculated from these measurements can be correlated with the sheet resistance of the samples. Sheet resistance is found to decrease with increasing $\langle PosG \rangle$ value due to the increased charge carrier concentration of the samples. Sheet resistance values of ≈ 100 Ω/sq were produced for a wide range of $\langle PosG \rangle$ values, demonstrating that only partial doping may be required to reduce the sheet resistance of graphene films by an order of magnitude. This may also indicate that the presence of holes and the quality of the graphene was a limiting factor to reducing the films' sheet resistance. These results show $FeCl_3$-FLG to be ideally suited for use as a transparent conducting electrode, with the versatility to be employed on flexible substrates with negligible detriment to its electrical or optical properties.[18]

4. CONCLUSIONS

$FeCl_3$-FLG shows great promise to the photovoltaics community for its applications as a transparent conductive electrode as well as for its potential use in flexible devices. We have demonstrated an improved method for the transfer of large area graphene samples, as well as introducing a new metric by which to characterize the chemical doping in these samples. The need for uniform, high quality CVD graphene in order to produce $FeCl_3$-FLG samples with homogeneous charge carrier concentrations was highlighted by the variation of $\langle PosG \rangle$ with flake thickness. Further optimization of intercalation conditions is required to improve large area $FeCl_3$-FLG properties beyond a sheet resistance of 100 Ω/sq. However, this sheet resistance value is still low enough to make $FeCl_3$-FLG an attractive flexible electrode, ideal for the production of flexible photovoltaic devices based around organic photovoltaic materials, or even other 2D materials such as Transition Metal Dicalchogenides. This offers potential for a new generation of flexible photovoltaic devices, with broadened applications as well as improved efficiencies compared to those made with inferior electrodes.

ACKNOWLEDGMENTS

REFERENCES

[1] Furchi, M. M., Zechmeister, A. A., Hoeller, F., Wachter, S., Pospischil, A., and Mueller, T., "Photovoltaics in Van der Waals Heterostructures," *IEEE Journal on Selected Topics in Quantum Electronics* **23**(1) (2017).

[2] Furchi, M. M., Pospischil, A., Libisch, F., Burgdo, J., and Mueller, T., "Photovoltaic Effect in an Electrically Tunable van der Waals Heterojunction," **14**(8), 4785–4791 (2014).

[3] Britnell, L., Ribeiro, R. M., Eckmann, A., Jalil, R., Belle, B. D., Mishchenko, A., Kim, Y., Gorbachev, R. V., Georgiou, T., Morozov, S. V., Grigorenko, A. N., Geim, A. K., Casiraghi, C., Neto, A. H. C., and Novoselov, K. S., "Strong Light-Matter Interactions Thin Films," **340**(6138), 1311–1315 (2013).

[4] Li, X. S., Zhu, Y. W., Cai, W. W., Borysiak, M., Han, B. Y., Chen, D., Piner, R. D., Colombo, L., and Ruoff, R. S., "Transfer of Large-Area Graphene Films for High-Performance Transparent Conductive Electrodes," *Nano Letters* **9**(12), 4359–4363 (2009).

[5] Brus, V. V., Gluba, M. A., Zhang, X., Hinrichs, K., Rappich, J., and Nickel, N. H., "Stability of graphene-silicon heterostructure solar cells," *Physica Status Solidi (A) Applications and Materials Science* **211**(4), 843–847 (2014).

[6] Espinosa, N., García-Valverde, R., Urbina, A., and Krebs, F. C., "A life cycle analysis of polymer solar cell modules prepared using roll-to-roll methods under ambient conditions," *Solar Energy Materials and Solar Cells* **95**(5), 1293–1302 (2011).

[7] Wu, X., Xu, H., Wang, Y., Rogach, A. L., Shen, Y., and Zhao, N., "General observation of the memory effect in metal-insulator-ITO structures due to indium diffusion," *Advanced Materials* **19**(20), 3364–3367 (2007).

[8] Gallardo, D. E., Bertoni, C., Dunn, S., Gaponik, N., and Eychmüller, A., "Cathodic and anodic material diffusion in polymer/semiconductor-nanocrystal composite devices," *Advanced Materials* **19**(20), 3364–3367 (2007).

[9] Nair, R. R., Blake, P., Grigorenko, A. N., Novoselov, K. S., Booth, T. J., Stauber, T., Peres, N. M. R., and Geim, A. K., "Fine Structure Constant Defines Visual Transparency of Graphene," *Science* **320**(5881), 1308–1308 (2008).

[10] Khrapach, I., Withers, F., Bointon, T. H., Polyushkin, D. K., Barnes, W. L., Russo, S., and Craciun, M. F., "Novel highly conductive and transparent graphene-based conductors," *Advanced Materials* **24**(21), 2844–2849 (2012).

[11] Dresselhaus, M. S. and Dresselhaus, G., "Advances in Physics Intercalation compounds of graphite," *Advances in Physics* **51**(1), 1–186 (1981).

[12] Bointon, T. H., Jones, G. F., De Sanctis, A., Hill-Pearce, R., Craciun, M. F., and Russo, S., "Large-area functionalized CVD graphene for work function matched transparent electrodes.," *Scientific reports* **5**, 16464 (2015).

[13] Sanctis, A. D., Jones, G. F., Townsend, N. J., Craciun, M. F., Russo, S., Sanctis, A. D., Jones, G. F., Townsend, N. J., and Craciun, M. F., "thin optoelectronic devices An integrated and multi-purpose microscope for the characterization of atomically thin optoelectronic devices," *Review of Scientific Instruments* **88** (2017).

[14] Lazzeri, M. and Mauri, F., "Nonadiabatic Kohn anomaly in a doped graphene monolayer," *Physical Review Letters* **97**(26), 29–32 (2006).

[15] Zhan, D., Sun, L., Ni, Z. H., Liu, L., Fan, X. F., Wang, Y., Yu, T., Lam, Y. M., Huang, W., and Shen, Z. X., "FeCl3-based few-layer graphene intercalation compounds: Single linear dispersion electronic band structure and strong charge transfer doping," *Advanced Functional Materials* **20**(20), 3504–3509 (2010).

[16] Pisana, S., Lazzeri, M., Casiraghi, C., Novoselov, K. S., Geim, A. K., Ferrari, A. C., and Mauri, F., "Breakdown of the adiabatic Born-Oppenheimer approximation in graphene.," *Nature materials* **6**(3), 198–201 (2007).

[17] Zhang, Y., Gomez, L., Ishikawa, F. N., Madaria, A., Ryu, K., Wang, C., Badmaev, A., and Zhou, C., "Comparison of graphene growth on single-crystalline and polycrystalline Ni by chemical vapor deposition," *Journal of Physical Chemistry Letters* **1**(20), 3101–3107 (2010).

[18] Torres Alonso, E., Karkera, G., Jones, G. F., Craciun, M. F., and Russo, S., "Homogeneously Bright, Flexible, and Foldable Lighting Devices with Functionalized Graphene Electrodes," *ACS Applied Materials and Interfaces* **8**(26), 16541–16545 (2016).